

Article

# Warm Rain Analysis from Remote Sensing Data in the Metropolitan Area of Barcelona for 2015–2022

Tomeu Rigo 

Servei Meteorològic de Catalunya, Berlin St, 38–46, PO 08029 Barcelona, Spain; tomeu.rigo@gencat.cat

**Abstract:** The Metropolitan Area of Barcelona is one of the most densely populated European regions. The hydrological conditions are very extreme, as are those of the Mediterranean Basin, with long drought periods. The management of water systems is one of the priorities, implying the understanding of the whole life cycle of water. One of the worst-known steps in this cycle corresponds to the rainfall events occurring between warm and cold periods, with quasi-tropical precipitation but with little or no lightning activity. This manuscript relies on the analysis of this type of precipitation for 2015–2022 for characterization and modelling to provide the signatures that can help diagnose these events in real time. The comparison of cold convective and warm rain events through radar, lightning and numerical weather prediction data has allowed us to find the main differences between both types. Warm rain events are predominant in the region, with more than 70% cases exceeding 10 mm of daily precipitation. The maritime influence is crucial in most of the warm rain episodes.

**Keywords:** coastal region; catalonia; warm rain; thunderstorms; weather radar; lightning location sensors; freezing level



**Citation:** Rigo, T. Warm Rain Analysis from Remote Sensing Data in the Metropolitan Area of Barcelona for 2015–2022. *Hydrology* **2023**, *10*, 142. <https://doi.org/10.3390/hydrology10070142>

Academic Editor: Aristoteles Tegos

Received: 30 April 2023

Revised: 3 July 2023

Accepted: 3 July 2023

Published: 6 July 2023



**Copyright:** © 2023 by the author. Licensee MDPI, Basel, Switzerland. This article is an open access article distributed under the terms and conditions of the Creative Commons Attribution (CC BY) license (<https://creativecommons.org/licenses/by/4.0/>).

## 1. Introduction

The high spatiotemporal variability of rainfall plays a dominant role in hydrologic processes, according to Anagnostou et al. [1]. There is more variability and it has more incidence in regions such as the Mediterranean Basin, including Catalonia (the Region of Study), as many authors have presented before (e.g., [2–5]). This issue is of high importance at the time of managing the different resources associated with the life cycle of water, as the rivers, the settle, or the run-off [6–8]. Castillo and Rigo [9,10] showed this high variability of the precipitation regimes in the region of study through the comparison of radar fields and the lightning discharges detected.

Warm rain is a type of precipitation studied for years (see, for instance, the state-of-the-art preliminary research presented by Ogura et al. [11]). It refers to precipitation derived from processes in clouds without ice phase [12,13]. Rauber et al. [14] showed that warm rain could occur in clouds with temperatures close to  $-10^{\circ}\text{C}$  at the top. There are still some facets of warm rain micro-physics that remain not well understood by the scientific community. Lau and Wu [12] found that warm rain accounts for 31% of the total rain amount in the Tropics. Furthermore, Beard and Ochs [13] indicated that warm rain is also possible in mid-latitudes. Since the end of the 1960s, many cloud physicists have studied the interactions and processes inside the warm-rain-producing clouds [11].

Ogura et al. [11] (and later Beard and Ochs [13]) summarized that the distribution of sizes in the hydro-meteors is a combination of condensation, evaporation, coalescence, sedimentation, and break up. Takahashi described part of the dynamics of the process in his analysis of the initiation of clouds in Hawaii [15]. The clouds developed near the windward coastline in a scenario of air subsidence that produced a strong inversion in the first three km. This inversion limited cloud development to less than 3 km. One of the interesting observations was that the development of the cloud was better developed in the upper part than in the base (where drop growth occurs) when strong winds occur

near the inversion layer. The humidity and the local convergence were the main elements contributing to the droplets' growth in the cloud base. Furthermore, the rainfall efficiency doubles with an increase in the Sea Surface Temperature (SST) of 6 °C [12]. Another element that contributes to the warm rain processes is the presence of cloud condensation nuclei (CCN), which are more abundant in continental clouds than maritime, implying that droplets have a larger size in the last case [13]. In this context, Reborá et al. [16] found that warm rain events in mid-latitudes were of short duration and, on the other hand, accumulations of precipitation that usually exceed multi-centennial return periods. These authors also found that warm rain occurs in situations with low values of Convective Available Potential Energy (CAPE), and the coastline can play a dominant role in the modelling of the event.

Remote sensing (weather radar, lightning registers, and satellite imagery) has evolved as the best way to analyze precipitating clouds in general and warm rain production and their micro-physics, in particular, [17]. Many projects have studied the precipitation in different regions or for the whole globe through different types of satellites (e.g., [18,19]). Anagnostou et al. [1] evaluated some satellite products for the mid-latitudes using data from tropical missions, providing errors in the estimations for different precipitation types. Atlas et al. [20] determined that there is no well-defined relationship between reflectivity and rainfall intensity for any of the range of classes of precipitation, which are highly dependent on the various processes occurring during drop formation. Muller et al. [21] combined many remote sensing sources (radar, satellite, and spectro-photometry) to model the indirect effects of aerosols on clouds. The comparison between continental and maritime events indicated that the first ones contain fewer smaller droplets and a high number of large droplets, indicating the melting of frozen hydro-meteors in continental cases.

With respect to weather radar, Caylor and Illingworth [22] found that in warm rain initiation, the first echoes showed the presence of few large raindrops, with concentrations of raindrops much lower than the detected during the mature stage. These observations were more evident in tropical regions, while in mid-latitudes, freezing could occur after warm rain initiation. Lightning detection in warm-rain events has allowed us to observe that electrification of clouds is more usual over land than over the ocean because the first is usually hotter than the sea surface, influencing the conditional instability and the updraft strength [23–25]. Furthermore, the coarse spray associated with the sea also inhibits lightning occurrence.

Some of the previous references noted that the warm rain characteristics differ depending on whether it occurs over land or the sea, in the tropics or in the mid-latitudes. Thurai et al. [26] identified some events with stratiform and convective rainfall in the southeastern United States coastal region, in which warm rain occurred in some periods, but the detection with weather radar was not as simple as in the tropical cases. Kumar et al. [27] obtained similar results but for South America, a region with a marked influence of the Andes range. Moving to the Mediterranean Sea, we must remark the research of Khain et al. in the Eastern Basin [28–30], and of Reborá et al. [16] in the Western Basin. Probably, the most remarkable result found by Khain et al. is that warm rain initiates faster over the sea than over land because of the presence of large drops, and furthermore, that sea-ground temperature difference and the location and intensity of the breeze front play dominant roles in the initiation of the warm rain events.

In Catalonia and the other regions of the western Mediterranean Basin, only one research work refers to warm rain. The analysis of six events by Ballart et al. [31], three of warm rain and three of deep convection, showed similar results to the previous: no clear synoptic pattern, convergence lines, high values of differences of temperature between sea and land and between 850 hPa and surface, most of the precipitable water mass concentrated in the lowest 4 km (inversion level), shallow vertical developments in radar profiles with weak signals in satellite imagery, moderate reflectivity radar values at low levels, and finally, few if any cloud-to-ground lightning flashes. Departing from all those previous features but focusing on the remote sensing data, the main goal of the present

research is the automatic identification of warm rain events in the Central Coast of Catalonia and, later, the characterization of all cases of high precipitations in the region of study.

## 2. Data and Methods

### 2.1. Region of Interest

The area considered in the research includes the land and sea zones inside the red rectangle (see left panel of Figure 1) with coordinates: 1.5° W, 2.7° W, 41.1° N, and 41.9° N. Most (67% of the total area, 8872 km<sup>2</sup>) of the selected region is land (brown shaded area in the right panel of Figure 1). Topography contrasts with heights between 0 and 1670 m and very steep terrain, as in most of the Mediterranean Basin. These high differences modulate the hydrology, with short rivers of fast time-response. This fact, combined with the large population density (with more than 3,300,000 inhabitants), creates the necessity of understanding of possible different rain regimes. Considering the difficulties of correctly forecasting and diagnosing warm rain events, it prioritises identifying all those elements that can help to improve the knowledge of this type of precipitation.

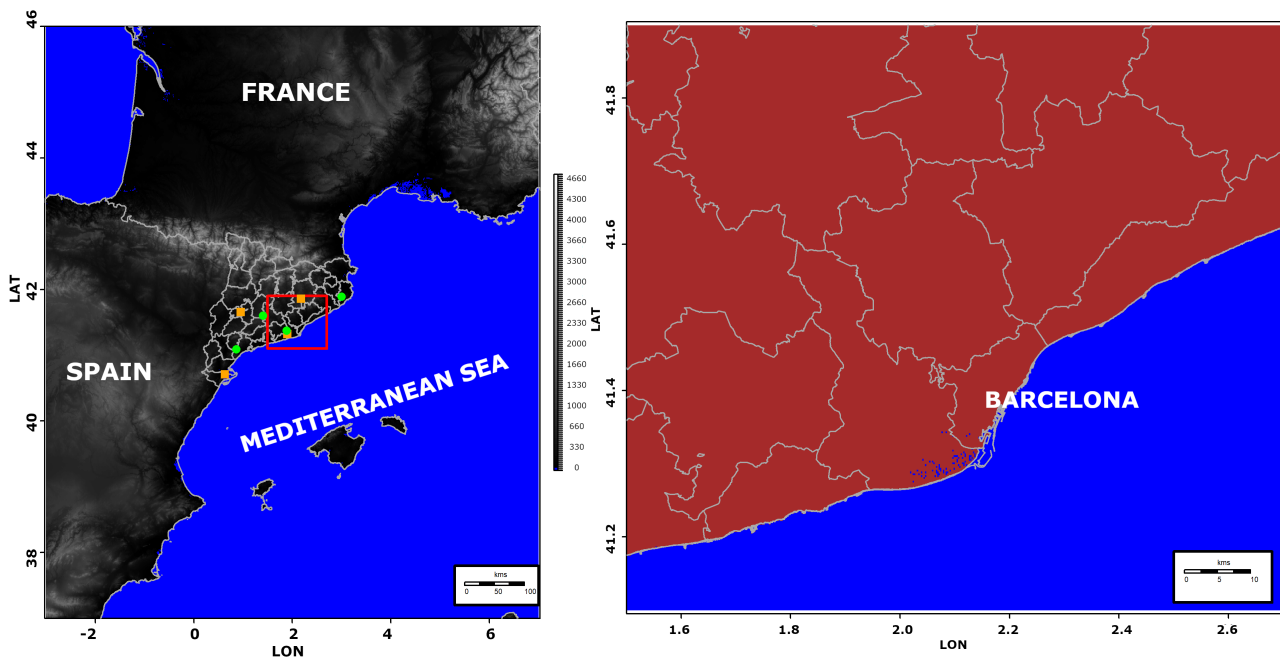


**Figure 1.** Left: map of the North-Western part of the Mediterranean Basin, centered in the region of study (red rectangle). Green and orange points indicate the locations of the sensors of the radar and lightning location networks, respectively. Right panel: Enlargement of the region of study, divided in two areas: land (brown shaded) and sea (blue shaded).

### 2.2. Data Used

The data belongs to the period 2015–2022 and has multiple sources, listed and described below:

- \* Radar data: the principal source of this research. The radar products have a time resolution of 6 min (except for the quantitative daily rainfall estimation) and a grid size of 1 km × 1 km. All the products are planar except the 3D CAPPI (Constant Altitude Plan Position Indicator) product, which consists of 40 planar fields with a height step of 0.5 km (from 0.5 to 20 km). Apart from the CAPPI, the other products are Echo Top of 12 dBZ reflectivity (TOP12) [32], and the 24 h Quantitative Precipitation Estimation (QPE) using radar and rain gauges of automatic weather stations [7,33]. Green points in the left panel of Figure 1 show the location of the different single-pol C-band radars of the Catalan network. The region of interest is well-covered by the composition products, with scarce affectation caused by beam blockage. It is

important to note that the QPE product is composed of radar and automatic weather station data, using geo-statistical techniques as it was introduced in [33]. That research showed that by combining both sources the QPE fields were very reliable because the new field introduces the quantitative information provided by rain gauges and the qualitative distribution of precipitation observed by radar. However, some recurrent electromagnetic signal interference has occurred for some periods, but the reflectivity values did not appear to disturb the radar fields during the precipitation events [34]. It is worthy to note that TOP12 has been selected because 12 dBZ is the threshold coinciding with the occurrence of 0.1 mm precipitation in the study region.

- \* Lightning detection: the lightning location system of the Servei Meteorològic de Catalunya provides the cloud-to-ground flashes (positive and negative) with a position accuracy error of less than 500 m in the region of interest because the distribution of the network's sensors (orange dots in the left panel of the Figure 1). Rigo et al. (2021) [10] has more information regarding these data.
- \* Freezing level fields: maps of the height of the freezing level derived from the operational running model of the Servei Meteorològic de Catalunya: the Weather Research and Forecasting (WRF) Model version 4.3. The configuration of the model consists of the parametrizations YSU (boundary layer), WSM5 (clouds microphysics), Kain-Fritsch (convection), RRTM (long-wave radiation), Dudhia (short-wave radiation), and Noah LSM (soil) [35]. The grid size of these fields is 1 km × 1 km, and the time resolution is three hours. These maps allow determining the part of the reflectivity structures exceeding the melting level height.

### 2.3. Methodology

#### 2.3.1. Description of the Precipitation Regimes

As the principal purpose of the research is to establish an automatic identification of warm rain events in the region of study (the Central Coast of Catalonia), the first step consists of the characterization of this regime type and differentiation of others, mainly cold convective rainfall episodes. Figure 2 shows two examples (22 August 2022 and 9 March 2022) for cases with warm rain regime: convective precipitation is characterized in radar fields by gradients in the reflectivity patterns (in both horizontal and vertical directions). However, the convection develops below or just few kilometres over the freezing level in the case of warm rain. The profiles shown in Figure 2 are for the 95th percentile at each level and time from the 3D CAPPis over each of the two regions (land and sea) presented in Figure 1 (right panel). The figure shows that vertical development can be higher, and the reflectivity intensity stronger over land or the sea depending on the event. The warm rain events are relatively short episodes (less than 6 h), with moderate to large values of reflectivity concentrated in the lower levels (the core does not usually exceed 5 kilometres, and the TOP12 rarely exceed the 7 km and no more than 4 km over the freezing level), and little to no lightning activity.

To compare with cold convective rainfall events, Figure 3 shows the same graphs for two other episodes: 18 August 2022 and 22 June 2022. In these two cases, the rainfall regime is very different, with TOP12 exceeding the freezing level by at least 8 km, with high values of reflectivity, and a period of cloud-to-ground lightning activity coinciding with the maximum reflectivity or the highest TOP12 values. On the other hand, this kind of event has a similitude with warm rain in the sense that the maximum can occur alternatively over land or sea. Finally, it is worth saying that cold convective rainfall events have very short peaks (no longer than 1 h), usually followed by long periods (up to 2 h) of moderate or weak reflectivity values, and little if any lightning activity.

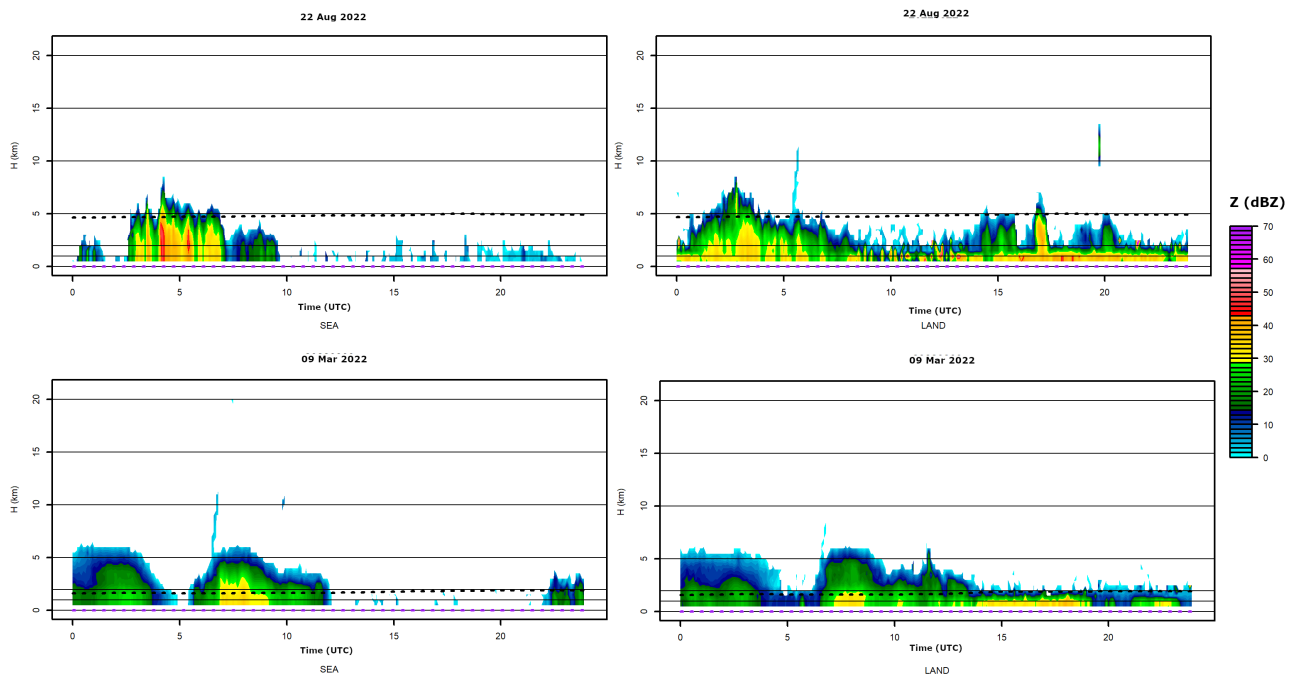


**Figure 2.** Vertical profile of reflectivity for the 95th percentile for the sea (left column) and land (right column) regions, for two episodes classified as warm rain: 22 August 2022 (top row) and 9 September 2022 (bottom row). The black dotted line indicated the 95th percentile of the freezing level height over land and sea regions (three hours intervals) and the purple dotted line shows the number of cloud-to-ground flashes in the same regions with hourly resolution.

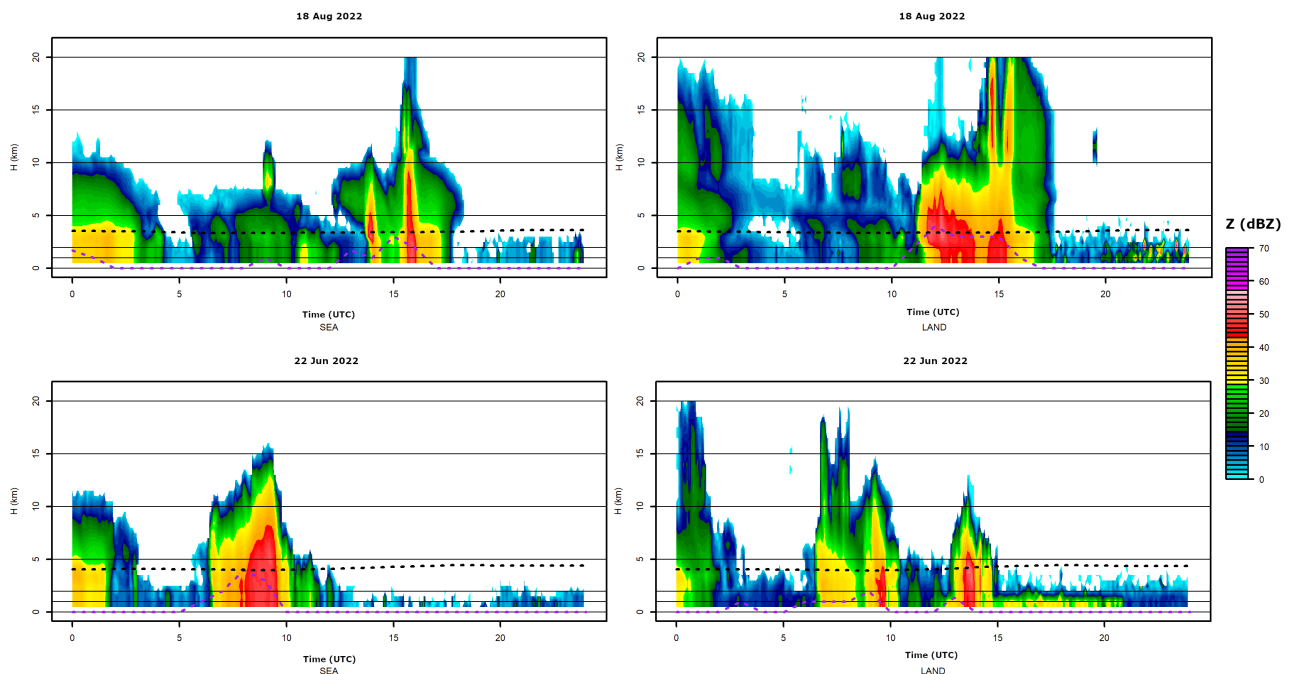


**Figure 3.** As in Figure 2, but for cold convective events (18 August 2022 and 22 June 2022).

### 2.3.2. Identification of the Precipitation Regimes

This project seeks to identify warm rain events through the evaluation of daily quantitative precipitation, lightning data, daily maximum TOP12, and the daily highest freezing level height fields. The following criteria have been applied:

1. Selecting those days with maximum precipitation estimated over 10 mm in the studied region. The event also should register a mean precipitation of 1 mm to avoid outliers.
2. Regarding cloud-to-ground flashes, the number of observations must be lower than ten during the event. If the number of flashes exceeds this threshold, the event is considered to be cold convective rain.

Then, the objective is to determine the differences between the TOP12 and the freezing level to better characterize both variables and determine the variations depending on different elements. Before moving to the results, it should go deeper into some considerations. The first one is that the freezing level does not vary in excess during the whole day (see black dotted lines in Figures 2 and 3). Analyzing two of the days previously presented, the eight daily fields do not show many differences with the maxima map, as can be observed in Figures 4 and 5.

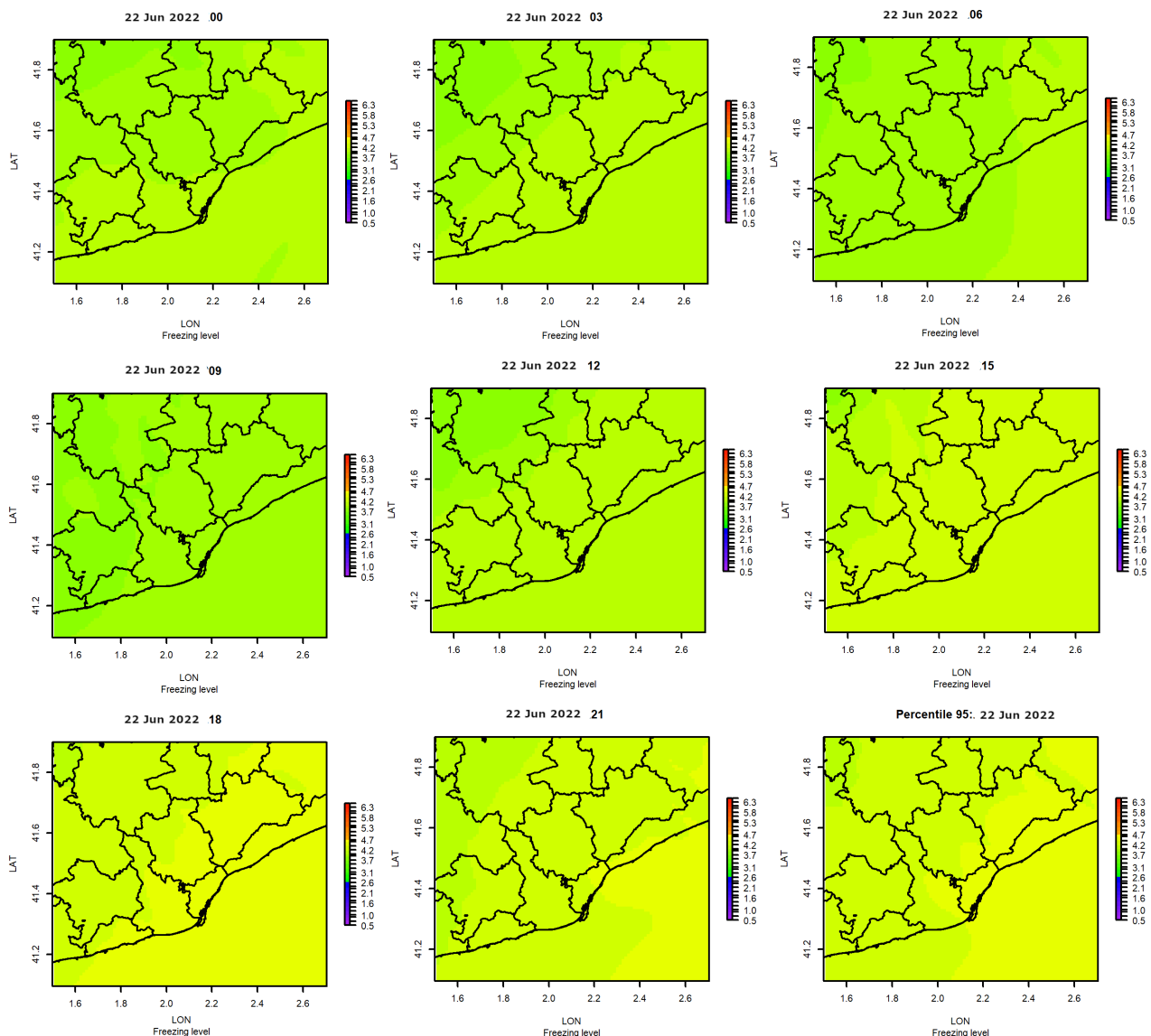


**Figure 4.** Maps of the evolution of freezing level for the cold convective rain event during the period 0000–2100 UTC 22 June 2022, and the maximum daily values (last chart, at bottom right).

For the cold convective rainfall event (Figure 4), freezing level heights moved between 3.5 and 4.5 km, while for the warm rain episode (Figure 5), the freezing level was between 4.2 and 5.3 km. From these, the following can be determined: first, that warm rain can occur

with the melting level height moving over a wide range, and second, that the freezing level ranges 1 km between daily maximum and minimum in the studied region.

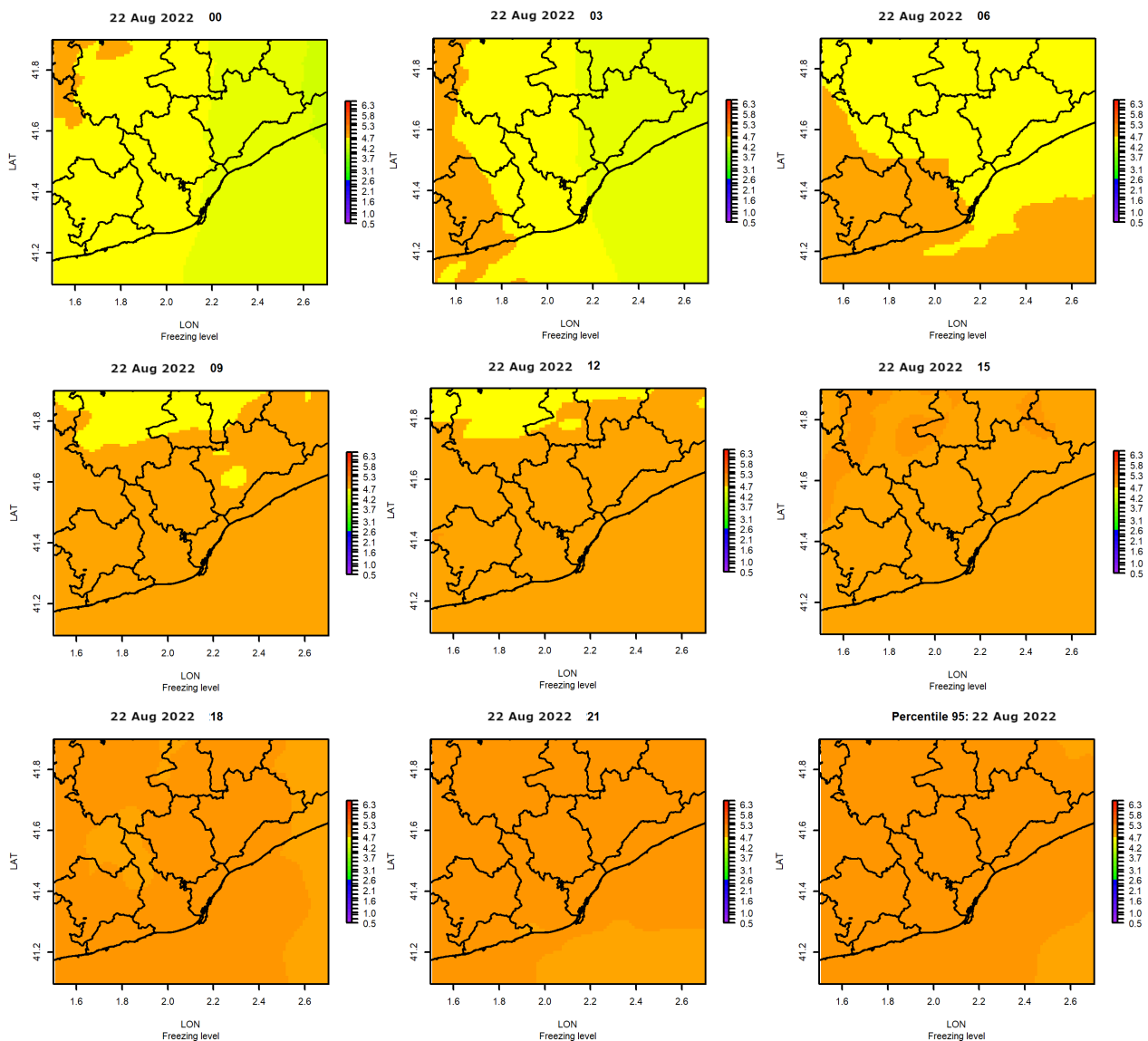


**Figure 5.** As in Figure 4 but for the warm rain event during the period 0000–2100 UTC 22 August 2022.

### 2.3.3. Homogeneity of the Fields for the Different Variables

Figure 6 summarizes the previous observations using the boxplot charts of the maximum freezing level fields of the four previously presented cases. In this case, the height variation is lower than the total daily, with differences of less than 500 m. Then, the selection of the 95th percentile, in this case, is not as relevant as for the rest of the magnitudes, which present a large spatial and temporal variability. Figure 6 also shows the differences in the freezing level height depending on the event, which can vary between 2 and 5 km.

In contrast to the homogeneous behaviour of the freezing level fields, radar fields have heterogeneous patterns, both in time and space. For instance, Figure 7 shows two cases of 95th daily TOP12 and total daily QPE for the 22 August 2022 and 9 March 2022 events. There is a good agreement between both fields and besides, there are notable differences in values along the studied area.

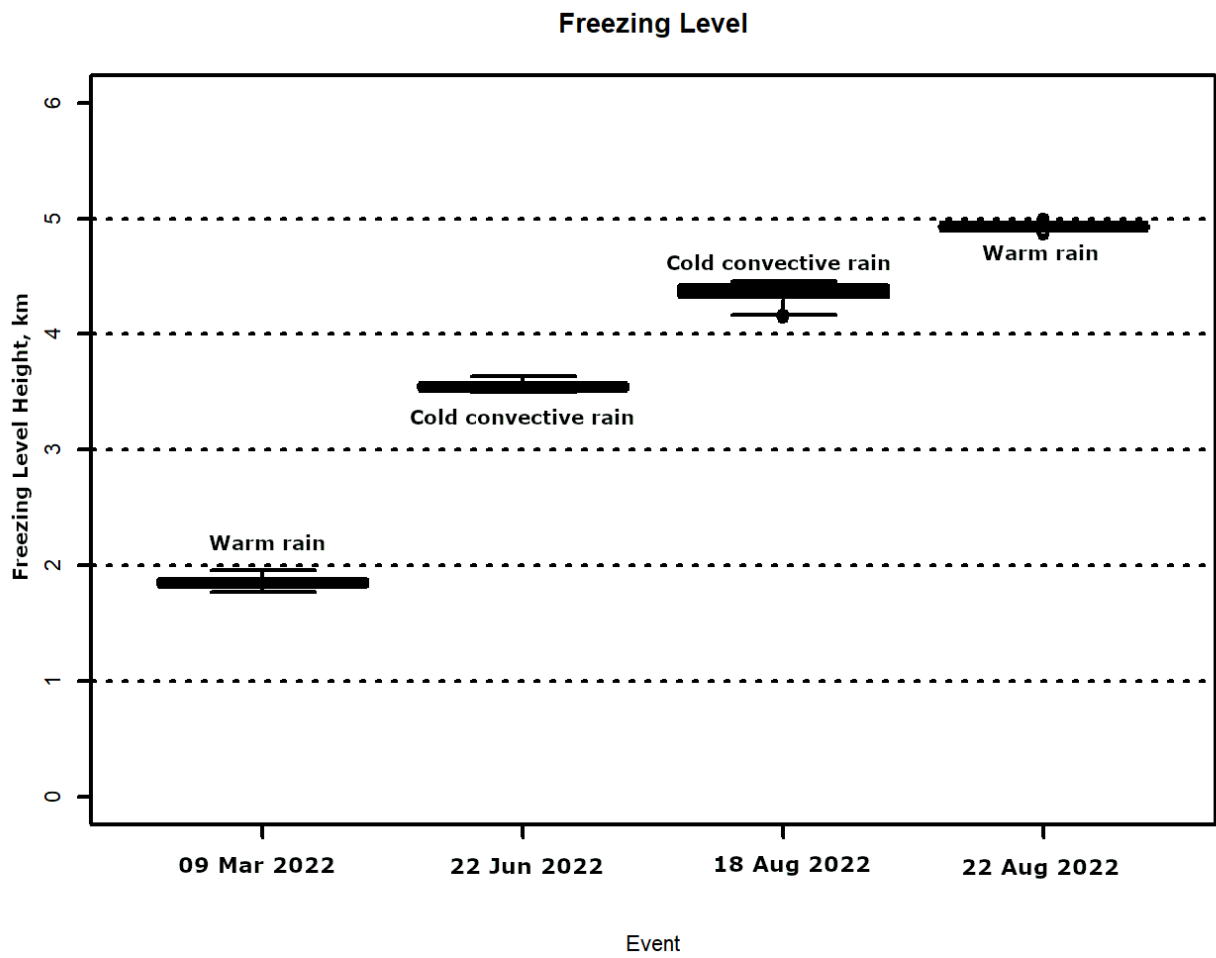


Figure 6. Boxplot of the daily maximum heights of the freezing level for the four previously selected events.

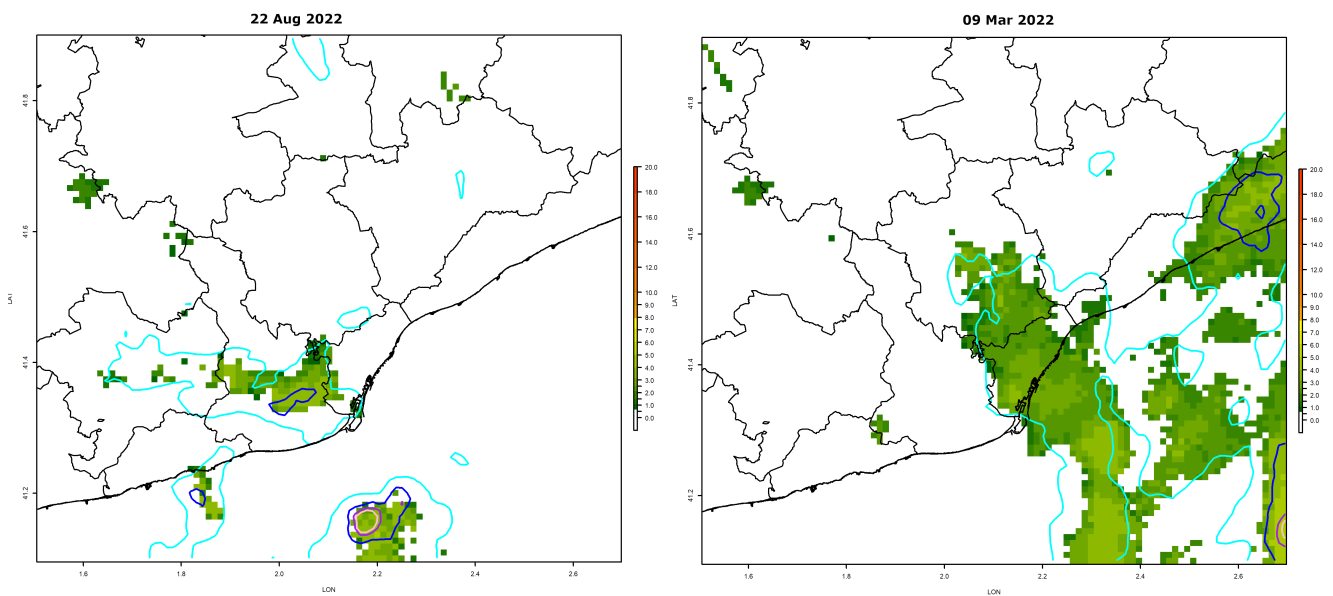
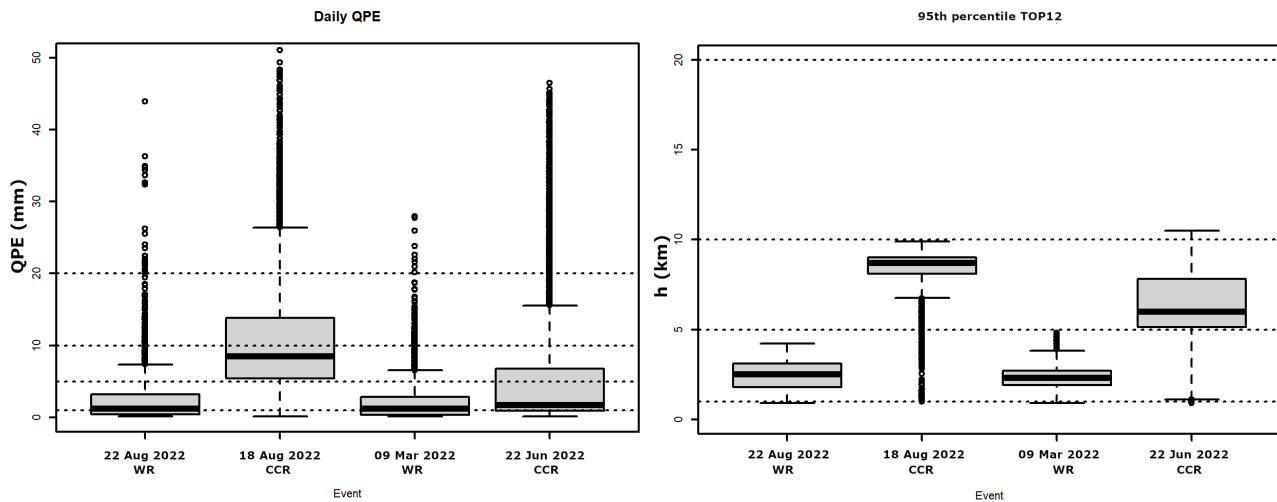


Figure 7. Daily maps of 95th percentile TOP12 (shaded areas) and daily QPE (colored lines) for the 22 August 2022 (left) and 9 March 2022 (right) events. Color lines of the QPE correspond to the 1 mm (cyan), 10 mm (blue), and 20 mm (purple) thresholds.

Figure 8 summarizes the differences between the different events for the daily QPE and the 95th percentile TOP12. These differences are more evident for QPE, but the TOP12 also presents an inhomogeneity, especially if compared with the freezing level boxplot (Figure 6). Because of this, it is interesting to select the 95th percentile as a threshold because of two reasons: first, it helps to remove the outliers caused by different anomalies in the radar fields, and second, it is a value closer to the maximum in most of the cases.



**Figure 8.** Boxplot of the daily QPE (left) and daily 95th percentile TOP12 (right) for the four events presented in Figures 2 and 3. WR indicates warm rain event and CCR means cold convective rain case.

#### 2.3.4. Characterization of the Precipitation Regimes

Once all the rain events (exceeding 10 mm) of the period 2015 to 2022 have been labelled according to the lightning activity (warm or cold convective), each one has been characterized depending on the location of the maximum (over land or sea), the month of the year, and the differences between the TOP12 and the freezing level.

### 3. Results

There were 540 events in which rainfall exceeded 10 mm. Three hundred and ninety-four (72.96%) events were classified as WR, during which there were fewer than 10 cloud-to-ground lightning flashes. The remaining 146 (27.04%) were classified as CCR, characterized by 10 or more cloud-to-ground lightning flashes. The final characterization of the events should allow for better discrimination of each type of event.

#### 3.1. Monthly Distribution

Figure 9 summarizes the seasonal behaviour of the two types of events. CCR events were most frequent in September, with secondary maxima during August and October. Deep convection is usually common during those months in the region of study leading to short but intense precipitation episodes, as indicated, for instance, in [7]. Some of the CCR events during these months included severe convective weather (hail, strong straight-line winds, tornadoes) [36–38].

On the other hand, WR events peaked during April and September, with secondary maxima during March and May, as well as August and October. Del Moral et al. [39] showed, for a closed coastal area in the South of Catalonia, that most of these events are characterized by shallow convection, developed over the sea and moving over the land recursively, generating a convective train effect [40]. The relationship between this distribution and the previous observations leads to identifying the high contribution of mesoscale convective systems for the first maximum [41].

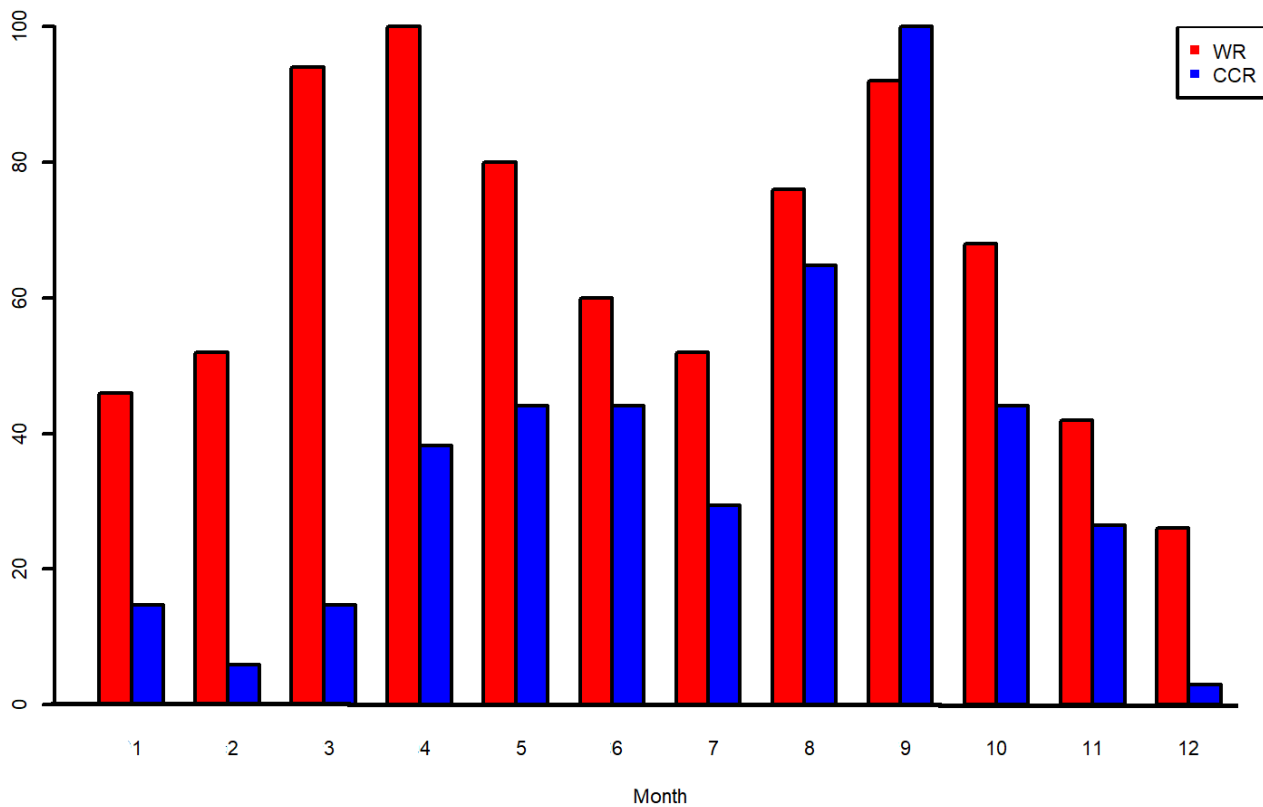


**Figure 9.** Normalized monthly distributions of the WR (red) and CCR (blue) events.

### 3.2. Relationship between the Vertical Development of the Radar Echoes and the Freezing Level

The vertical development of the reflectivity plays a principal role in cloud-to-ground lightning generation, as stated by Salvador et al. [42]. This is because the strong updrafts that lead to ice formation when the droplets exceed the freezing level height favour charge separation inside the cloud. In the case of WR, freezing is not usual and thus lightning occurrence is lower. This step of the research has consisted in comparing CCR and WR events through the difference between the daily 95th percentiles of the TOP12 and the freezing level height (from the WRF model). The higher the difference between TOP12 and the freezing level, the more possible is the existence of precipitating water in solid state inside the cloud (associated with CCR events).

In the case of CCR events, Figure 10 shows the variation of the difference between heights throughout the year. The maximum is clearly in July (mean value of 6 km), with also significant differences (over 5 km) between May and November. The case of January is an anomaly caused by a few events that occurred during 2018. In any case, events with significant lightning activity require differences exceeding 4 km.

By contrast, the WR events have an inverse distribution of the difference between TOP12 and the freezing level. In WR events (Figure 11), the minimum values occur in those July and August, with values close to 1 km. These are the months when the difference in TOP12 and freezing level heights is maximized for CCR events, coinciding with both the warmer season and the more unstable atmospheric conditions [41,43]. In the other months, especially the colder ones (November, December, January, and February), the height difference can be higher, reaching 3 km.

To sum up, the difference between the vertical development of the precipitating structures and the freezing level is what limits the occurrence of lightning activity, as opposed to the absolute values of both magnitudes.

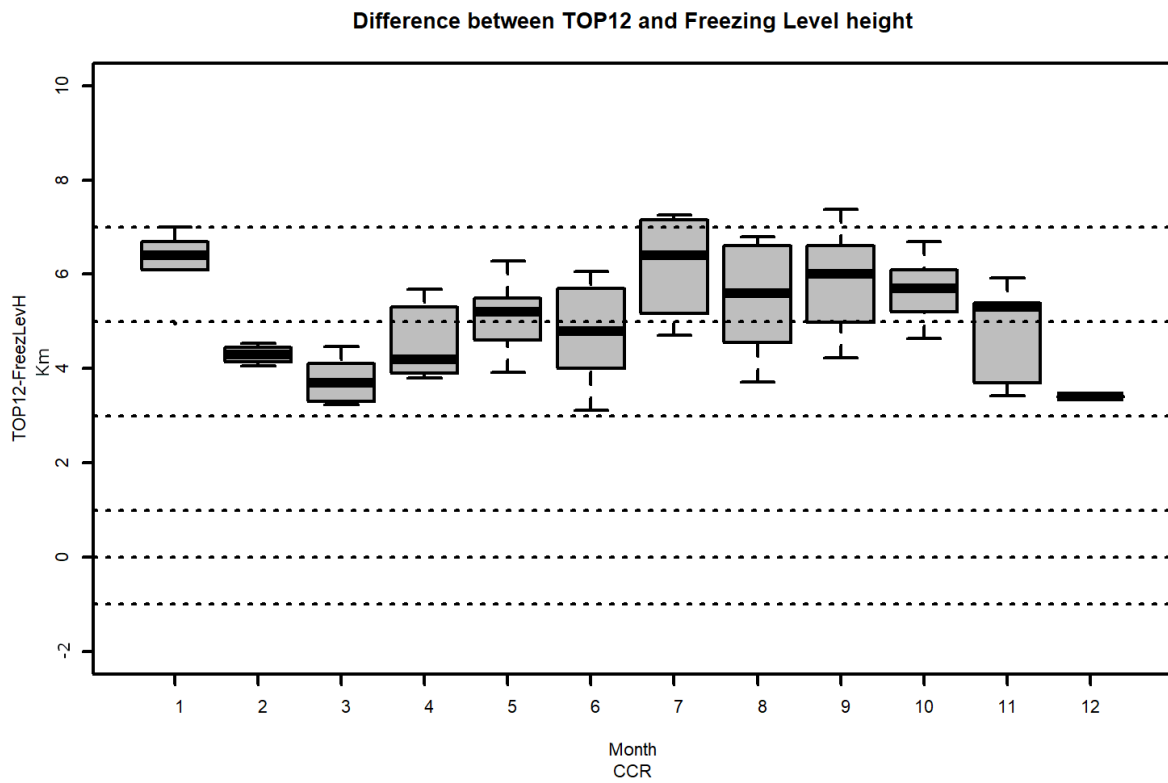


Figure 10. Normalized monthly distributions of the difference between the daily 95th percentiles of the TOP12 and of the freezing level height in the case of CCR events.

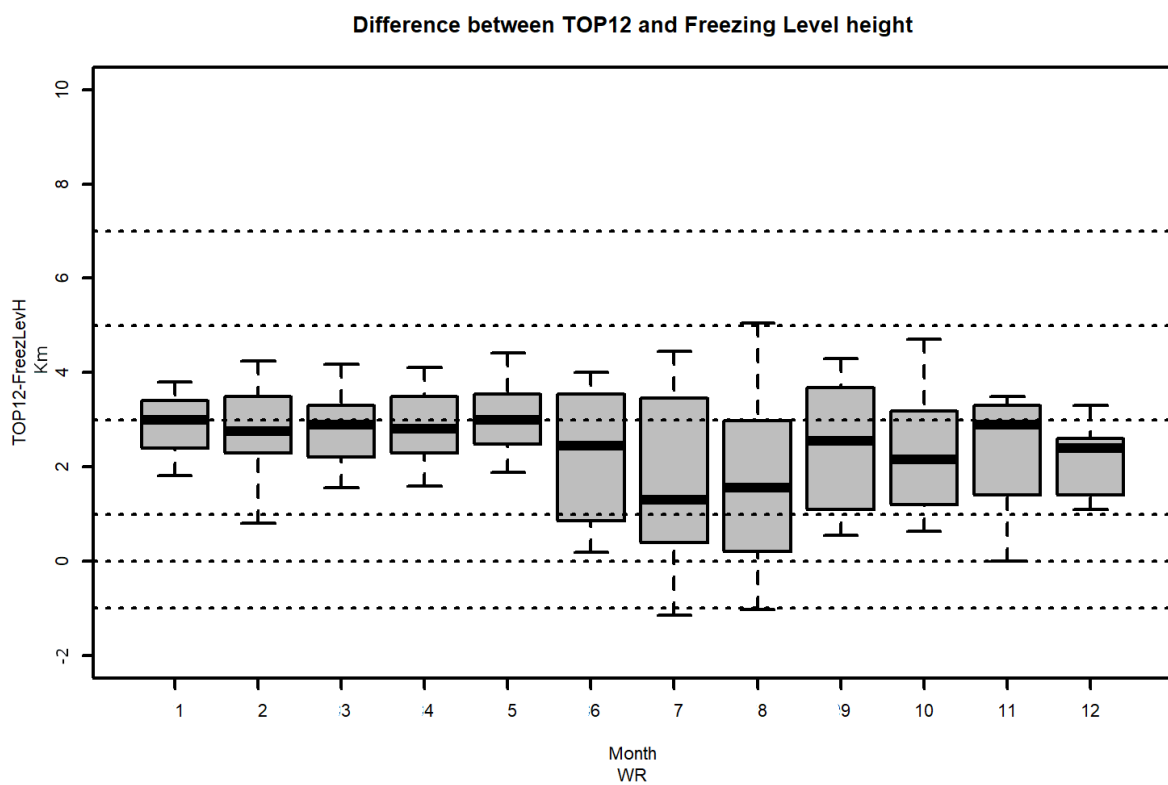
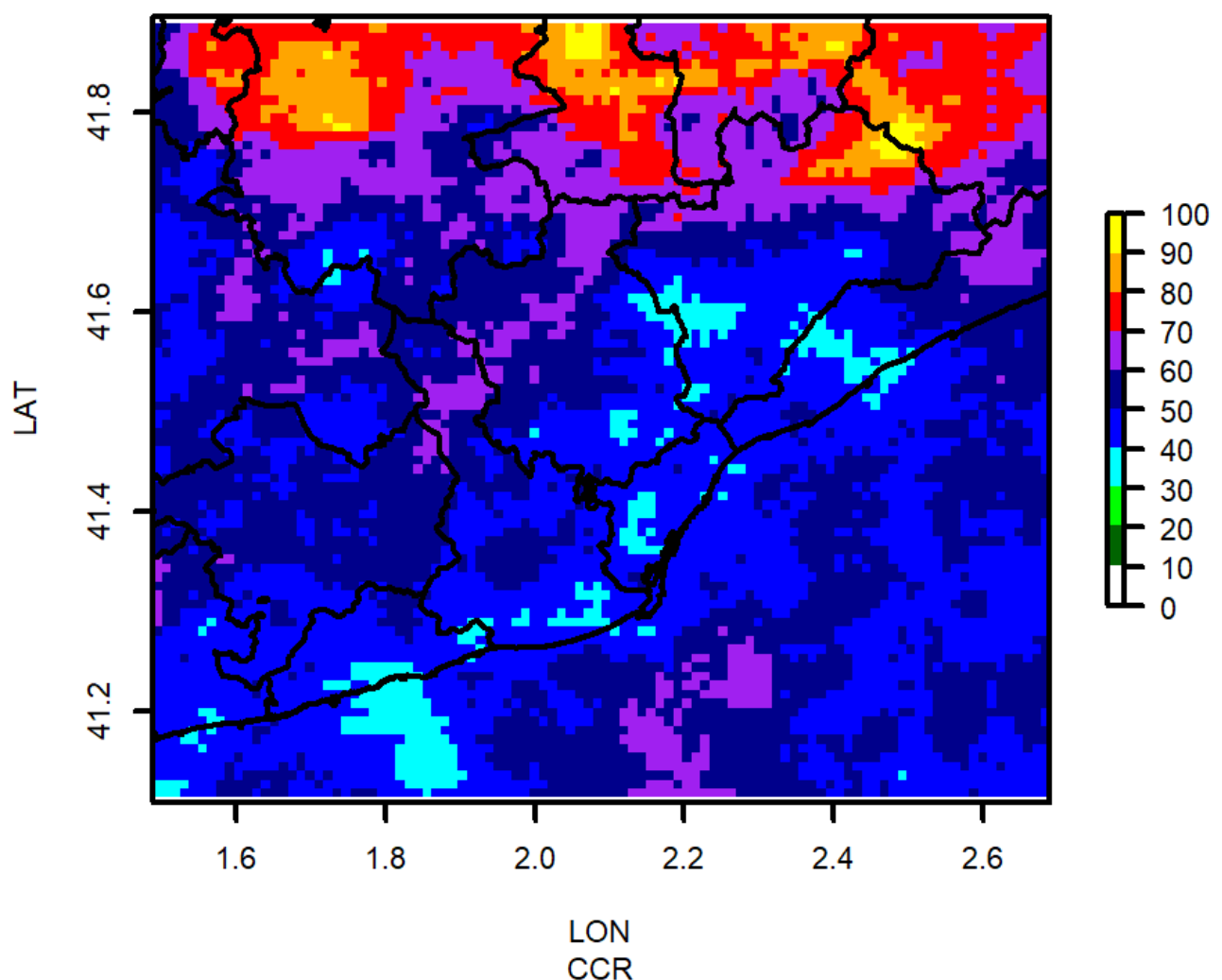


Figure 11. As the Figure 10 for the WR events.

### 3.3. Spatial Distribution of Precipitation

The last step of this research has consisted of the identification of the hot spots of precipitation, depending on the type of precipitation regime. Figures 12 and 13 present the normalized spatial distribution of pixels with 10 mm or more of daily QPE for the region of study between 2015 and 2022. In the case of CCR (Figure 12), the distribution of maxima shows a clear peak in the inland area (north of the image), indicating that most of the convective events come from the North and the maritime influence is low. There are two secondary hot spots with sea influence: one in the Eastern part, between 41.60 and 41.70° N Latitude and 2.55 and 2.65° E Longitude, and the second over the sea, in the bottom-middle of the map. By contrast, there is a minimum belt along the coastal area.

#### Cases with more than 10 mm



**Figure 12.** Normalized spatial distribution of events exceeding the 10 mm of daily QPE for the CCR.

The distribution for the WR is opposite to the CCR one, with a larger influence of the sea: the sea maximum has increased, and it has the same importance that the land maximum in relation to CCR events, which has reduced in extension and focused on the northeastern portion of the study region. In the middle are some secondary hot spots between land and sea, while a minimum is observed in the western part of the region of study.

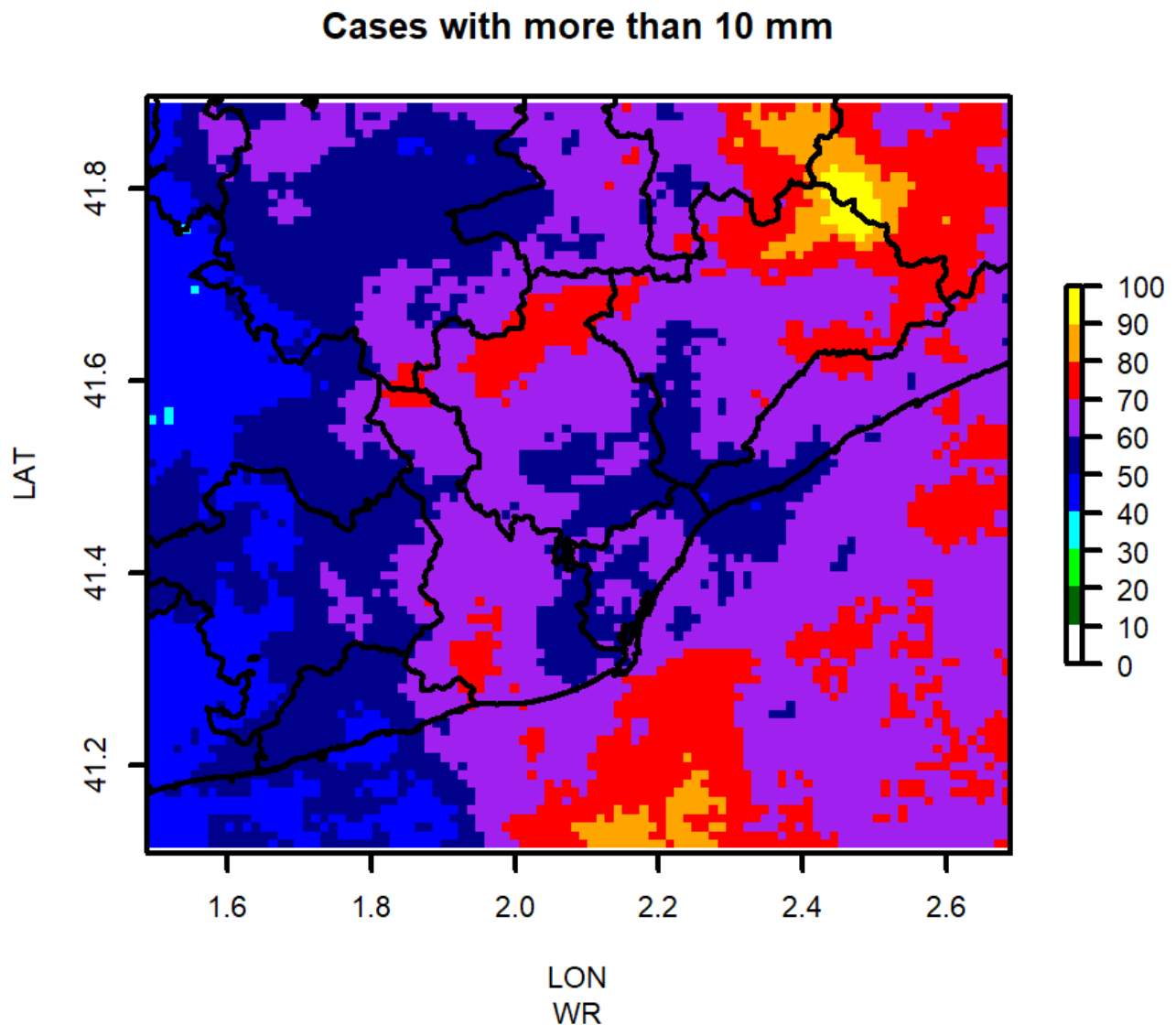


**Figure 13.** As the Figure 12 for the WR events.

#### 4. Discussion and Conclusions

The Central Coast of Catalonia suffers the same effects as the rest of the Mediterranean Basin, with the succession of drought and wet periods. The last ones usually produce events of intense rainfalls and floods, as stated by Llasat et al. [44,45]. These conditions have been dramatically accentuated in the last decades, by a combination of a high population density (one of the largest in Europe) pressure and the effects of global warming, which are more evident in these latitudes. Because of this, managing the water life cycle is more necessary than ever, to minimise the lack of water and to manage the water needs of the different sectors: agriculture, industry, energy, and tourism, among others.

The present research focuses on the analysis of a type of event, the Warm Rain, that is well-known in many regions of the world, mainly the Tropics, but has been poorly explored in the coastal of Catalonia. The analysis has focused on the characterization of the WR and CCR events in the region using weather radar, lightning data, and the freezing level height derived from the WRF model. The first point has been the identification of the events, based on the definitions found in the bibliography: CCR and WR usually produce large rain accumulations (in this case, the daily threshold was 10 mm) but the difference is the occurrence of lightning activity (moderate to large for CCR and little if any for WR events). Three-dimensional time evolution of the reflectivity fields over land and sea has allowed

the observation of some characteristics of the rainfall patterns in events that satisfy the previous definitions: the vertical development, with larger gradient and height in the case of the CCR events, and the evolution in time of the precipitating structures, with longer periods of rainfall in the case of WR.

The first result is that WR has high importance in this area, considering the number of cases (more than 70% of the total of cases with more than 10 mm of daily QPE during the studied period). Furthermore, the monthly distribution is different for the two types: single-modal maximum centred on September in the case of CCR and bi-modal maxima (April and September) for WR. Another interesting result is the differences in the height of the vertical development of the rainfall structures (TOP12) and the freezing level: the values are notably higher in the case of CCR in general (5 km, versus 2 km for WR events), and in particular between July and August (with differences of 6 km and 1 km, respectively). These results are very coincident with studies that focused on particular cases or general precipitation [7,41,42,44,45]. Finally, the maritime influence in the WR events is clearer than for the CCR, according to the spatial distribution of the cases. This result is in general in agreement with previous studies [19,23,26].

An interesting future project could be the comparison of the results of the current research with the data provided by the GPM (Global Precipitation Model) Mission. In fact, the radar network of the Servei Meteorològic de Catalunya acted as super-site for validating GPM data in the past [46].

**Funding:** This research received no external funding.

**Data Availability Statement:** Data is available under requirement via e-mail to the Author.

**Acknowledgments:** The author wants to thank to his colleagues of the Servei Meteorològic de Catalonia for their valuable comments that have helped to improve the quality of the manuscript.

**Conflicts of Interest:** The author declares no conflict of interest.

### Abbreviations

The following abbreviations are used in this manuscript:

SST	Sea Surface Temperature
CCN	Cloud Condensation Nuclei
CAPE	Convective Available Potential Energy
CAPPI	Constant Altitude Plan Position Indicator
TOP12	Echo Top of 12 dBZ reflectivity
QPE	24 h Quantitative Precipitation Estimation
CCR	Cold Convective Rainfall event
WR	Warm Rain event
WRF	Weather Research and Forecasting
SMC	Servei Meteorològic de Catalunya (in Catalan, Meteorological Service of Catalonia)

### References

1. Anagnostou, E.N.; Maggioni, V.; Nikolopoulos, E.I.; Meskele, T.; Hossain, F.; Papadopoulos, A. Benchmarking high-resolution global satellite rainfall products to radar and rain-gauge rainfall estimates. *IEEE Trans. Geosci. Remote Sens.* **2009**, *48*, 1667–1683. [[CrossRef](#)]
2. Lana, X.; Martínez, M.; Serra, C.; Burgueno, A. Spatial and temporal variability of the daily rainfall regime in Catalonia (northeastern Spain), 1950–2000. *Int. J. Climatol. J. R. Meteorol. Soc.* **2004**, *24*, 613–641. [[CrossRef](#)]
3. Lopez-Bustins, J.A.; Lemus-Canovas, M. The influence of the Western Mediterranean Oscillation upon the spatio-temporal variability of precipitation over Catalonia (northeastern of the Iberian Peninsula). *Atmos. Res.* **2020**, *236*, 104819. [[CrossRef](#)]
4. Turco, M.; Llasat, M. Trends in indices of daily precipitation extremes in Catalonia (NE Spain), 1951–2003. *Nat. Hazards Earth Syst. Sci.* **2011**, *11*, 3213–3226. [[CrossRef](#)]
5. Llasat, M.C.; Marcos, R.; Turco, M.; Gilibert, J.; Llasat-Botija, M. Trends in flash flood events versus convective precipitation in the Mediterranean region: The case of Catalonia. *J. Hydrol.* **2016**, *541*, 24–37. [[CrossRef](#)]

6. Parés, M.; Brugué, Q.; Espluga, J.; Miralles, J.; Ballester, A. The strengths and weaknesses of deliberation on river basin management planning: Analysing the water framework directive implementation in Catalonia (Spain). *Environ. Policy Gov.* **2015**, *25*, 97–110. [[CrossRef](#)]
7. Esbrí, L.; Rigo, T.; Llasat, M.C.; Aznar, B. Identifying Storm Hotspots and the Most Unsettled Areas in Barcelona by Analysing Significant Rainfall Episodes from 2013 to 2018. *Water* **2021**, *13*, 1730. [[CrossRef](#)]
8. Gilabert, J.; Tardà, A.; Llasat, M.; Corbera, J. Assessment of local climate zones over metropolitan area of barcelona and added value of urban atlas, corine land cover and copernicus layers under Inspire specifications. *Urban Clim.* **2016**, *17*, 116–134.
9. Castillo, S.; Rigo, T.; Farnell, C. Can the Correlation between Radar and Cloud-to-Ground Daily Fields Help to Identify the Different Rainfall Regimes? The Case of Catalonia. *Atmosphere* **2022**, *13*, 808. [[CrossRef](#)]
10. Rigo, T.; Castillo, S. Evolution of Radar and Lightning Variables in Convective Events in Barcelona and Surroundings for the Period 2006–2020. *Adv. Environ. Eng. Res.* **2021**, *2*, 1–18. [[CrossRef](#)]
11. Ogura, Y.; Takahashi, T. The development of warm rain in a cumulus model. *J. Atmos. Sci.* **1973**, *30*, 262–277. [[CrossRef](#)]
12. Lau, K.; Wu, H. Warm rain processes over tropical oceans and climate implications. *Geophys. Res. Lett.* **2003**, *30*. [[CrossRef](#)]
13. Beard, K.V.; Ochs, H.T., III. Warm-rain initiation: An overview of microphysical mechanisms. *J. Appl. Meteorol. Climatol.* **1993**, *32*, 608–625. [[CrossRef](#)]
14. Rauber, R.M.; Olthoff, L.S.; Ramamurthy, M.K.; Kunkel, K.E. The relative importance of warm rain and melting processes in freezing precipitation events. *J. Appl. Meteorol.* **2000**, *39*, 1185–1195. [[CrossRef](#)]
15. Takahashi, T. Warm rain study in Hawaii—Rain initiation. *J. Atmos. Sci.* **1981**, *38*, 347–369. [[CrossRef](#)]
16. Rebora, N.; Molini, L.; Casella, E.; Comellas, A.; Fiori, E.; Pignone, F.; Siccardi, F.; Silvestro, F.; Tanelli, S.; Parodi, A. Extreme rainfall in the Mediterranean: What can we learn from observations? *J. Hydrometeorol.* **2013**, *14*, 906–922. [[CrossRef](#)]
17. Testik, F.; Barros, A.P. Toward elucidating the microstructure of warm rainfall: A survey. *Rev. Geophys.* **2007**, *45*. [[CrossRef](#)]
18. Stephens, G.L.; Haynes, J.M. Near global observations of the warm rain coalescence process. *Geophys. Res. Lett.* **2007**, *34*. [[CrossRef](#)]
19. Prat, O.P.; Nelson, B.R. Characteristics of annual, seasonal, and diurnal precipitation in the Southeastern United States derived from long-term remotely sensed data. *Atmos. Res.* **2014**, *144*, 4–20. [[CrossRef](#)]
20. Atlas, D.; Ulbrich, C. Drop size spectra and integral remote sensing parameters in the transition from convective to stratiform rain. *Geophys. Res. Lett.* **2006**, *33*. [[CrossRef](#)]
21. Muller, C.L.; Kidd, C.; Fairchild, I.J.; Baker, A. Investigation into clouds and precipitation over an urban area using micro rain radars, satellite remote sensing and fluorescence spectrophotometry. *Atmos. Res.* **2010**, *96*, 241–255. [[CrossRef](#)]
22. Caylor, I.; Illingworth, A. Radar observations and modelling of warm rain initiation. *Q. J. R. Meteorol. Soc.* **1987**, *113*, 1171–1191. [[CrossRef](#)]
23. Williams, E.; Stanfill, S. The physical origin of the land–ocean contrast in lightning activity. *C. R. Phys.* **2002**, *3*, 1277–1292. [[CrossRef](#)]
24. Pan, Z.; Mao, F.; Rosenfeld, D.; Zhu, Y.; Zang, L.; Lu, X.; Thornton, J.A.; Holzworth, R.H.; Yin, J.; Efrim, A.; et al. Coarse sea spray inhibits lightning. *Nat. Commun.* **2022**, *13*, 4289. [[CrossRef](#)]
25. Liou, Y.A.; Kar, S. Study of cloud-to-ground lightning and precipitation and their seasonal and geographical characteristics over Taiwan. *Atmos. Res.* **2010**, *95*, 115–122. [[CrossRef](#)]
26. Thurai, M.; Bringi, V.; Wolff, D.; Marks, D.; Pabla, C. Testing the drop-size distribution-based separation of stratiform and convective rain using radar and disdrometer data from a mid-latitude coastal region. *Atmosphere* **2021**, *12*, 392. [[CrossRef](#)]
27. Kumar, S.; Moya-Álvarez, A.S.; Castillo-Velarde, C.D.; Martínez-Castro, D.; Silva, Y. Effect of low-level flow and Andes mountain on the tropical and mid-latitude precipitating cloud systems: GPM observations. *Theor. Appl. Climatol.* **2020**, *141*, 157–172. [[CrossRef](#)]
28. Khain, A.P.; Rosenfeld, D.; Sednev, I. Coastal effects in the Eastern Mediterranean as seen from experiments using a cloud ensemble model with detailed description of warm and ice microphysical processes. *Atmos. Res.* **1993**, *30*, 295–319. [[CrossRef](#)]
29. Khain, A.P.; Sednev, I. Simulation of precipitation formation in the Eastern Mediterranean coastal zone using a spectral microphysics cloud ensemble model. *Atmos. Res.* **1996**, *43*, 77–110. [[CrossRef](#)]
30. Khain, A.; Rosenfeld, D.; Pokrovsky, A.; Blahak, U.; Ryzhkov, A. The role of CCN in precipitation and hail in a mid-latitude storm as seen in simulations using a spectral (bin) microphysics model in a 2D dynamic frame. *Atmos. Res.* **2011**, *99*, 129–146. [[CrossRef](#)]
31. Ballart, D.; Figuerola, F.; Aran, M.; Rigo, T. Analysis of warm convective rain events in Catalonia. In Proceedings of the 11th Plinius Conference on Mediterranean Storms, Barcelona, Spain, 7–11 September 2009; p. Plinius11.
32. Rigo, T.; Farnell Barqué, C. Evaluation of the Radar Echo Tops in Catalonia: Relationship with Severe Weather. *Remote Sens.* **2022**, *14*, 6265. [[CrossRef](#)]
33. Rigo, T.; Llasat, M.C.; Esbrí, L. The Results of Applying Different Methodologies to 10 Years of Quantitative Precipitation Estimation in Catalonia Using Weather Radar. *Geomatics* **2021**, *1*, 347–368. [[CrossRef](#)]
34. Altube, P.; Bech, J.; Argemí, O.; Rigo, T.; Pineda, N. Intercomparison and potential synergies of three methods for weather radar antenna pointing assessment. *J. Atmos. Ocean. Technol.* **2016**, *33*, 331–343. [[CrossRef](#)]
35. Mercader Carbó, J.; Codina, B.; Sairouni, A.; Cunillera, J. Results of the meteorological model WRF-ARW over Catalonia, using different parameterizations of convection and cloud microphysics. *Tethys J. Mediterr. Meteorol. Climatol.* **2010**, *7*, 75–86. [[CrossRef](#)]

36. Rodríguez, O.; Bech, J.; Arús, J.; Castán, S.; Figuerola, F.; Rigo, T. An overview of tornado and waterspout events in Catalonia (2000–2019). *Atmos. Res.* **2021**, *250*, 105415. [[CrossRef](#)]
37. Bech, J.; Pascual, R.; Rigo, T.; Pineda, N.; López, J.; Arús, J.; Gayá, M. An observational study of the 7 September 2005 Barcelona tornado outbreak. *Nat. Hazards Earth Syst. Sci.* **2007**, *7*, 129–139. [[CrossRef](#)]
38. Farnell, C.; Rigo, T. The Lightning Jump, the 2018 “Picking up Hailstones” Campaign and a Climatological Analysis for Catalonia for the 2006–2018 Period. *Tethys* **2020**, *17*, 10–20. [[CrossRef](#)]
39. del Moral, A.; del Carmen Llasat, M.; Rigo, T. Connecting flash flood events with radar-derived convective storm characteristics on the northwestern Mediterranean coast: Knowing the present for better future scenarios adaptation. *Atmos. Res.* **2020**, *238*, 104863. [[CrossRef](#)]
40. Doswell, C.A., III; Brooks, H.E.; Maddox, R.A. Flash flood forecasting: An ingredients-based methodology. *Weather Forecast.* **1996**, *11*, 560–581. [[CrossRef](#)]
41. Rigo, T.; Berenguer, M.; del Carmen Llasat, M. An improved analysis of mesoscale convective systems in the western Mediterranean using weather radar. *Atmos. Res.* **2019**, *227*, 147–156. [[CrossRef](#)]
42. Salvador, A.; Pineda, N.; Montanyà, J.; López, J.A.; Solà, G. Thunderstorm charge structures favouring cloud-to-ground lightning. *Atmos. Res.* **2021**, *257*, 105577. [[CrossRef](#)]
43. Rigo, T.; Pineda, N.; Bech, J. Analysis of warm season thunderstorms using an object-oriented tracking method based on radar and total lightning data. *Nat. Hazards Earth Syst. Sci.* **2010**, *10*, 1881–1893. [[CrossRef](#)]
44. Llasat, M.d.C.; López, L.; Barnolas, M.; Llasat-Botija, M. Flash-floods in Catalonia: The social perception in a context of changing vulnerability. *Adv. Geosci.* **2008**, *17*, 63–70. [[CrossRef](#)]
45. Llasat, M.; Llasat-Botija, M.; Rodríguez, A.; Lindbergh, S. Flash floods in Catalonia: A recurrent situation. *Adv. Geosci.* **2010**, *26*, 105–111. [[CrossRef](#)]
46. Bech, J.; Vilaclara, E.; Pineda, N.; Rigo, T.; López, J.; O’Hora, F.; Lorente, J.; Sempere, D.; Fàbregas, F. The weather radar network of the Catalan Meteorological Service: Description and applications. In Proceedings of the ERAD, Visby, Sweden, 6–10 September 2004; Volume 2, pp. 416–420.

**Disclaimer/Publisher’s Note:** The statements, opinions and data contained in all publications are solely those of the individual author(s) and contributor(s) and not of MDPI and/or the editor(s). MDPI and/or the editor(s) disclaim responsibility for any injury to people or property resulting from any ideas, methods, instructions or products referred to in the content.